

# The clumpy torus around type II AGN as revealed by X-ray fluorescent lines

Jiren Liu<sup>1,\*</sup>, Yuan Liu<sup>2</sup>, Xiaobo Li<sup>2</sup>, Weiwei Xu<sup>1</sup>, Lijun Gou<sup>1</sup>, and Cheng Cheng<sup>1</sup>

<sup>1</sup>National Astronomical Observatories, 20A Datun Road, Beijing 100012, China

<sup>2</sup>Institute of High Energy Physics, Chinese Academy of Science, P.O. Box 918-3, Beijing 100049, China

## ABSTRACT

The reflection spectrum of the torus around AGN is characterized by X-ray fluorescent lines, which are most prominent for type II AGN. A clumpy torus allows photons reflected from the back-side of the torus to leak through the front free-of-obscuraton regions. Therefore, the observed X-ray fluorescent lines are sensitive to the clumpiness of the torus. We analyse a sample of type II AGN observed with *Chandra* HETGS, and measure the fluxes for the Si  $K\alpha$  and Fe  $K\alpha$  lines. The measured Fe  $K\alpha$ /Si  $K\alpha$  ratios, spanning a range between 5–60, are far smaller than the ratios predicted from simulations of smooth tori, indicating that the tori of the studied sources have clumpy distributions rather than smooth ones. Compared with simulation results of clumpy tori with a half-opening angle of  $60^\circ$ , the Circinus galaxy has a Fe  $K\alpha$ /Si  $K\alpha$  ratio of  $\sim 60$ , which is close to the simulation results for  $N = 5$ , where  $N$  is the average number of clumps along the line of sight. The Fe  $K\alpha$ /Si  $K\alpha$  ratios of the other sources are all below the simulation results for  $N = 2$ . Overall, it shows that the non-Fe fluorescent lines in the soft X-ray band are a potentially powerful probe of the clumpiness of the torus around AGN.

**Key words:** galaxies: Seyfert – galaxies: individual: (Circinus, Mrk 3, NGC 1068, NGC 3393, NGC 7582, NGC 2992, NGC 4388, NGC 4507, 3C 445) – X-rays: galaxies

## 1 INTRODUCTION

The obscuring torus around active galactic nucleus (AGN) is the key ingredient to unifying different types of AGN (e.g. Antonucci 1993). The distribution of matter in the torus was considered to be clumpy in early theoretical studies (Krolik & Begelman 1988). This implies that the classification of AGN is a probability of direct view of AGN (Elitzur 2008). The dust in the torus absorbs the radiation from the central AGN and re-radiates it in the infrared. While the simplified smooth model of torus was studied from early on, many detailed infrared observations point to clumpy distributions (see Hönig 2013; Netzer 2015, for recent reviews).

The clumpy nature of the torus is also supported by X-ray absorption variations on timescales from days to years. Different from dust emission in the infrared, obscuration of X-ray photons can be produced by dust-free gas within the sublimation radius. An extreme example is NGC 1365, which shows an occultation of the central AGN within 2 days, indicating that the obscuring clouds are located at similar distances to those of the broad line region (BLR, Risaliti et al. 2007). Statistical study of eclipse events in the *RXTE* (Rossi X-ray Timing Explorer) archive data by Markowitz et al.

(2014) showed that most of the clouds are located in the outer portion of the BLR. Recent hard X-ray monitoring of NGC 1068 by *NuSTAR* (Nuclear Spectroscopic Telescope Array) reveals flux variations above 20 keV, which imply a transition of the column density from  $10^{25} \text{ cm}^{-2}$  to  $6.7 \times 10^{24} \text{ cm}^{-2}$  (Marinucci et al. 2016). There seems to be a continuous distribution of clouds from the BLR to the parsec-scale torus (e.g. Bianchi et al. 2012; Netzer 2015).

X-ray spectra of type II AGN with column densities larger than  $10^{23} \text{ cm}^{-2}$  are particularly suitable for the study of the torus, since their intrinsic continua are heavily obscured in the soft X-ray band. This is especially true for Compton-thick AGN (with column densities  $> 1.2 \times 10^{24} \text{ cm}^{-2}$ ), the intrinsic continua of which are heavily suppressed below 10 keV, and the observed spectra are dominated by reflection emission from the torus (e.g. Comastri 2004). A characteristic feature of the reflection spectrum is the prominent Fe  $K\alpha$  emission line at 6.4 keV, which generally has an equivalent width (EW)  $\sim 1 \text{ keV}$  for Compton-thick AGN (e.g. Levenson et al. 2002).

A general feature of a clumpy torus is that soft X-ray photons, reflected from the back-side of the torus, are not significantly reduced due to their passage through the front free-of-obscuraton regions between clumps (Nandra & Geoge 1994; Yaqoob 2012; Liu & Li 2014). As shown by recent simulations, a clumpy torus provides significantly more soft X-ray photons than a smooth one

\* E-mail: jirenliu@nao.cas.cn

**Table 1.** List of the selected type II AGN observed with *Chandra* HETGS

Name	I(Si $K\alpha$ )	I(Mg XII Ly $\beta$ )	I <sub>c</sub> (Si $K\alpha$ )	I(Fe $K\alpha$ )	I(Fe)/I <sub>c</sub> (Si)	EW(Fe $K\alpha$ )	$N_{\text{H}}^T$	Reference of $N_{\text{H}}^T$
Circinus	$3.7 \pm 0.7$	$5.0 \pm 0.8$	$5.4 \pm 1.0$	$315.6 \pm 8.5$	$58 \pm 11$	1.6	8	Arévalo et al. (2014)
Mrk 3	$3.2 \pm 1.0$	$3.2 \pm 0.9$	$3.4 \pm 1.1$	$50.2 \pm 4.9$	$15 \pm 5$	0.46	0.9	Yaqoob et al. (2015)
NGC 1068	$6.4 \pm 1.5$	$18.4 \pm 3.0$	$6.4 \pm 1.5$	$43.6 \pm 5.6$	$7 \pm 2$	0.68	10	Bauer et al. (2015)
NGC 3393	$0.9 \pm 0.3$	$0.8 \pm 0.3$	$0.7 \pm 0.3$	$3.7 \pm 1.5$	$5 \pm 3$	0.56	2.2	Koss et al. (2015)
NGC 7582	$1.3 \pm 0.6$	$1.6 \pm 1.0$	$1.0 \pm 0.6$	$19.2 \pm 4.3$	$19 \pm 12$	0.39	3	Rivers et al. (2015)
NGC 2992	$2.5 \pm 0.9$	$2.4 \pm 1.1$	$2.0 \pm 0.9$	$18.8 \pm 4.9$	$9 \pm 5$	0.43	2	Xu et al. in prep
NGC 4388	$2.1 \pm 0.5$	$0.4 \pm 0.3$	$2.0 \pm 0.4$	$67.7 \pm 8.7$	$34 \pm 8$	0.17	0.4	Shirai et al. (2008)
NGC 4507	$1.7 \pm 0.6$	$1.9 \pm 0.6$	$1.3 \pm 0.6$	$55.5 \pm 11.4$	$43 \pm 22$	0.11	0.7	Marinucci et al. (2013)
3C 445	$0.7 \pm 0.2$	$0.6 \pm 0.3$	$0.6 \pm 0.2$	$16.1 \pm 4.1$	$27 \pm 11$	0.14	0.3	Braitto et al. (2011)

Note: I is the line intensity in units of  $10^{-6}$  photons  $\text{cm}^{-2} \text{s}^{-1}$  measured from the *Chandra* HEG data. I<sub>c</sub>(Si  $K\alpha$ ) is the value corrected for Galactic absorption (Circinus and Mrk 3) and the contribution of the Mg XII Ly $\beta$  line for other sources. EW(Fe  $K\alpha$ ) is in units of keV.  $N_{\text{H}}^T$  (in units of  $10^{24} \text{cm}^{-2}$ ) is the quoted column density of torus in recent literature. For NGC 2992, the Fe  $K\alpha$  line of the *Chandra* HEG spectrum has an EW  $\sim 0.4$  keV, which can be fitted with the scattered spectrum of the MYTorus model with a column density  $\sim 2 \times 10^{24} \text{cm}^{-2}$  (Xu et al. in prep).

when viewed edge-on, and the softer the photons, the larger the differences (Liu & Li 2014). The reflection spectrum can therefore be used to probe the matter distribution of the torus. For example, Bauer et al. (2015) found that a multiple-component reflector is needed to fit the *NuSTAR* spectra of NGC 1068. Baloković et al. (2014) found that the *NuSTAR* spectra of NGC 424, NGC 1320, and IC 2560 are better fitted with a "face-on" component of MYTorus model (Murphy & Yaqoob 2009), which was suggested to mimic the leakage of soft X-ray photons from a clumpy torus (Yaqoob 2012).

As the soft X-ray spectra of AGN are generally contaminated by other components, such as emission from photo-ionized gas, it is hard to measure the pure reflected continuum in the soft X-ray band. Instead, the non-Fe fluorescent lines (e.g. Si  $K\alpha$  line at 1.74 keV) emitted by the torus can be measured unambiguously, since they are unique line features that can not be confused with other components. Because the fraction of leaked photons depends on energy, the flux ratios of the Fe  $K\alpha$  line to non-Fe  $K\alpha$  lines would be a good probe of the matter distribution of the torus. The non-Fe fluorescent lines are generally weak, due to their small yields and relatively low abundances (e.g. Reynolds et al. 1994; Matt et al. 1997). Nevertheless, they are still observable, especially for Compton-thick AGN when the intrinsic continua are heavily suppressed (e.g. Xu et al. 2016).

In this Letter we compile a sample of type II AGN, observed with *Chandra* High Energy Transmission Grating Spectrometer (HETGS), to study their non-Fe fluorescent lines, focusing on the Si  $K\alpha$  line at 1.74 keV, which is generally the strongest of the non-Fe fluorescent lines. We compare the measured flux ratios of Fe  $K\alpha$ /Si  $K\alpha$  with simulation results of clump tori by Liu & Li (2014). The Fe  $K\alpha$ /Ni  $K\alpha$  ratio has been investigated previously (e.g. Molendi et al. 2003; Matt et al. 2004; Yaqoob & Murphy 2011). Note that the errors quoted are for the 90% confidence level.

## 2 OBSERVATIONAL DATA

The *Chandra* HETGS provides high resolution X-ray spectra for point-like sources (Canizares et al. 2005). It consists of a High Energy Grating (HEG) with a spectral resolution of 0.012 Å (full width half maximum, FWHM) and a Medium Energy Grating (MEG) with a resolution of 0.023 Å. The effective area of MEG is about 3 times larger than that of HEG around 1.74 keV, and drops

quickly above 6 keV. We searched the *Chandra* HETGS archive for type II AGN having sufficient signal-to-noise ratio (S/N) to allow a reliable measurement of the Si  $K\alpha$  line. We found a total of eight AGN, which are listed in Table 1. The Si  $K\alpha$  line is also detected in Cen A, but its dust lane complicates the estimation of the real flux of the Si  $K\alpha$  line and is therefore not included. Although classified as Seyfert 1.5, 3C 445 has an X-ray spectrum similar to type II AGN (e.g. Sambruna et al. 2007; Grandi et al. 2007) and has been included in the list. The first five sources listed in Table 1 are generally regarded as Compton-thick AGN, while the others are less obscured. Many of the selected sources have already been studied in the literature for their Fe  $K\alpha$  line (e.g. Shu et al. 2011).

We use the data downloaded from *Chandra* Transmission Grating Data Archive and Catalog (TGCat, Huenemoerder et al. 2011). All the spectra are extracted from a region with a 2 arcsec half-width in the cross-dispersion direction, and the  $\pm 1$  order data are combined together. The foreground Galactic absorption column density is  $6.2 \times 10^{21} \text{cm}^{-2}$  and  $1 \times 10^{21} \text{cm}^{-2}$  for Circinus and Mrk 3, respectively, and is negligible ( $< 0.7 \times 10^{21} \text{cm}^{-2}$ ) for other galaxies (Kalberla et al. 2005).

## 3 RESULTS

The Si  $K\alpha$  line (at 1.74 keV) is adjacent to the Mg XII Ly $\beta$  line at 1.745 keV. For Circinus, Mrk 3, and NGC 1068, their *Chandra* HEG data are deep enough to resolve the peaks of these two lines, thus allowing the two lines to be measured simultaneously. In particular, the line width of the Si  $K\alpha$  line can be measured with a spectral resolution 4 times better than that at 6.4 keV where the Fe  $K\alpha$  line resides. Measurements of the Si  $K\alpha$  line of Circinus, Mrk 3, and NGC 1068 were presented in Liu (2016). Si  $K\alpha$  line widths are 3 – 5 times smaller than those measured for the Fe  $K\alpha$  line, indicating that the line-emitting regions are outside the dust sublimation radius. We refer the reader to Liu (2016) for more details and for convenience, we have listed the relevant results in Table 1.

For all the other sources, the *Chandra* HEG data are not deep enough to allow a deblending of the Si  $K\alpha$  line and the Mg XII Ly $\beta$  line. The *Chandra* HEG spectra of these sources are shown in Fig. 1. It can be seen that the Si  $K\alpha$  line and the Mg XII Ly $\beta$  line are blended with each other. We fit the data with a model comprising one Gaussian line plus a power-law continuum. To improve the S/N ratio, the HEG and MEG data are fitted simultaneously. The fitting region is between 1.4 and 2.3 keV and neglecting the other

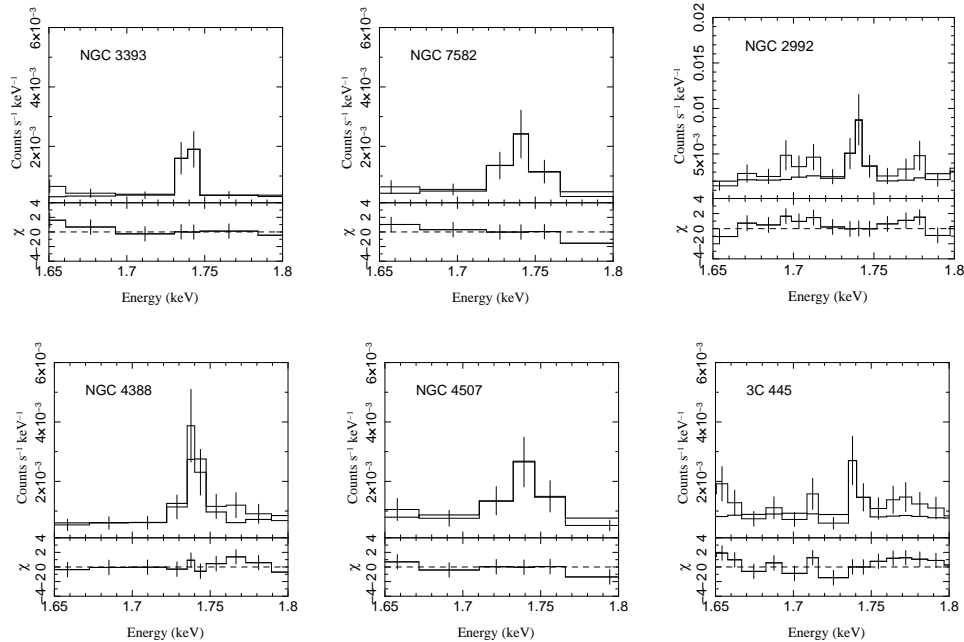


**Figure 1.** *Chandra* HEG spectra of the Si  $K\alpha$  line of the selected samples, except for Circinus, Mrk 3, and NGC 1068, whose spectra were presented in Liu (2016). The corresponding redshifts have been corrected. The data were binned to a minimum S/N ratio of 3. The fitted models of one Gaussian line plus a power-law continuum are plotted as the thick solid lines.

main emission features. The fitted results are plotted in Fig. 1 and listed in Table 1. We see that the one line model is sufficient to fit the data. If we replace the power-law continuum with a thermal continuum, the fitted intensities of Si  $K\alpha$  line are generally consistent with those of the power-law model, with differences smaller than 2%.

The contribution of the Mg XII Ly $\beta$  line can be estimated based on the fluxes of the Mg XII Ly $\alpha$  line at 1.472 keV, which are also listed in Table 1. For Circinus, Mrk 3, and NGC 1068, the fluxes of the Mg XII Ly $\beta$  line can be measured (Liu 2016) and the Mg XII Ly $\beta$ /Mg XII Ly $\alpha$  ratios (corrected for Galactic absorption) are  $0.38 \pm 0.11$ ,  $0.69 \pm 0.33$ , and  $0.19 \pm 0.07$ , respectively. For photo-ionized plasmas, the emissivity ratio between Mg XII Ly $\beta$  and Mg XII Ly $\alpha$  is around 0.1 – 0.25 (e.g. Kinkhabwala et al. 2003). Considering the uncertainties in the measurement, the Mg XII Ly $\beta$ /Mg XII Ly $\alpha$  ratios of Circinus and NGC 1068 are consistent with photo-ionization models. For Mrk 3, the ratio is larger than the predictions of photo-ionization models. It is likely that the Mg XII Ly $\beta$  line is over-estimated due to blending with the Si  $K\alpha$  line (Liu 2016). Assuming a ratio of Mg XII Ly $\beta$ /Mg XII Ly $\alpha$  of 0.2, the contribution of the Mg XII Ly $\beta$  line to the measured fluxes of Si  $K\alpha$  line is about 20% for all sources.

The fluxes of the Fe  $K\alpha$  line are measured using only the *Chandra* HEG data. We also adopt the model of one Gaussian line plus a power-law continuum. The fitting region is between 5 and 6.8 keV, and the measured fluxes are listed in Table 1. For reference, the EWs of the samples measured from the fitted models are also included. The measured EWs are generally larger than 0.3 keV, indicating the reflection-dominated nature of the X-ray spectra of the sample. From the measured fluxes of the Si  $K\alpha$  and Fe  $K\alpha$  line, we can calculate the Fe  $K\alpha$ /Si  $K\alpha$  ratio after correcting for the contribution of the Mg XII Ly $\beta$  line. The results are listed in Table 1. We see that they span a range between 5 – 60. The Circinus galaxy has

the largest Fe  $K\alpha$ /Si  $K\alpha$  ratio around 60, while the ratios of NGC 1068, NGC 3393, and NGC 2992 are as small as  $\sim 7$ .

Liu & Li (2014) simulated the reflection spectrum of a torus with clumpy distributions. The boundaries of the torus are defined by an inner radius of 0.1 pc, an outer radius of 2 pc, and a half-opening angle of  $60^\circ$ . This corresponds to a covering factor of 0.5 for a smooth torus. The clumpiness of the torus is described by the volume filling factor, the average number of clouds along the line of sight ( $N$ ), and the average column density ( $N_H$ ). The smaller the  $N$ , the more clumpy the torus. Liu & Li (2014) found that the filling factor only slightly affects the spectra, while  $N$  can change the emergent spectra significantly. A crude grid of  $N_H$  ( $10^{23}$ ,  $10^{24}$  and  $10^{25}$   $\text{cm}^{-2}$ ) and  $N$  (2, 5, 10) was simulated for a fixed photon index of  $\Gamma = 1.8$ . The simulated Fe  $K\alpha$ /Si  $K\alpha$  ratios for  $N_H = 10^{24}$   $\text{cm}^{-2}$  and  $10^{25}$   $\text{cm}^{-2}$  with a filling factor of 0.01 are plotted in Fig. 2. For comparison, the results of the smooth cases are also plotted.

First of all, we see that for the torus of  $N_H = 10^{24}$   $\text{cm}^{-2}$  with a smooth distribution, the Fe  $K\alpha$ /Si  $K\alpha$  ratio becomes smaller when the viewing angle changes from edge-on to face-on. This is due to less absorption of Si  $K\alpha$  photons in the face-on direction. For the clumpy torus, the Fe  $K\alpha$ /Si  $K\alpha$  ratio follows the same trend, but with a smaller value when viewed edge-on. The more clumpy the torus, the smaller the ratio. This is due to leakage of Si  $K\alpha$  photons as discussed in the Introduction. For the case of  $N_H = 10^{25}$   $\text{cm}^{-2}$ , the absorption becomes so severe that even no Si  $K\alpha$  photons appeared on some sight-lines. Nevertheless, the differences between the clumpy and smooth torus are similar to those for  $N_H = 10^{24}$   $\text{cm}^{-2}$ . The torus of  $N_H = 10^{25}$   $\text{cm}^{-2}$  is optically thick for Fe  $K\alpha$  photons, and the absorption of Fe  $K\alpha$  photons leads to a smaller Fe  $K\alpha$ /Si  $K\alpha$  ratio when viewed edge-on compared with the  $N_H = 10^{24}$   $\text{cm}^{-2}$  case. Note that, for  $N = 2$ , the Fe  $K\alpha$ /Si  $K\alpha$  ratios become almost isotropic, the effect of which was discussed in detail in Liu & Li (2014).

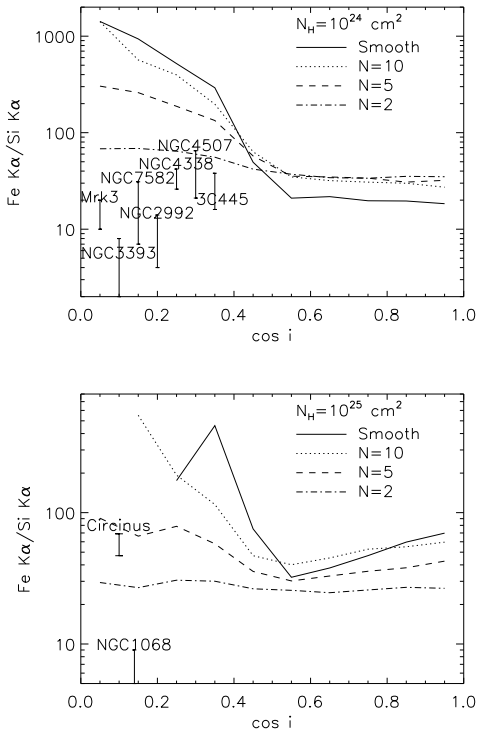


**Figure 2.** Fe  $K\alpha$ /Si  $K\alpha$  ratio against cosine of the inclination angle from simulations of clumpy tori with  $N_H = 10^{24} \text{ cm}^{-2}$  and  $10^{25} \text{ cm}^{-2}$  by Liu & Li (2014). The inclination angle  $0^\circ$  corresponds to face-on viewing, while  $90^\circ$  to edge-on.  $N$  is the average number of clouds along the line of sight, which is smaller for a more clumpy torus. The measured ratios are over-plotted according to their column densities, with an inclination angle arbitrarily assigned. Note that the measured ratios are all far below the predictions of the smooth torus, indicating that the tori of the samples have a clumpy distribution.

The measured Fe  $K\alpha$ /Si  $K\alpha$  line ratios are over-plotted in Fig. 2, either in the  $N_H = 10^{24} \text{ cm}^{-2}$  or the  $10^{25} \text{ cm}^{-2}$  panel, according to the column densities quoted in recent literature (shown in Table 1). The viewing angle is assigned with an arbitrary value larger than the half-opening angle of the simulated geometry. For the type II AGN studied here, to obscure the central AGN, the viewing angle must be larger than the half-opening angle of the torus. For Compton-thick sources, the reflection-dominated spectra indicate that they are most likely to be viewed edge-on. We see that all the measured Fe  $K\alpha$ /Si  $K\alpha$  ratios are far smaller than the predictions of the smooth torus with viewing angles larger than the half-opening angle of the torus. This indicates that the distribution of the tori of the sources is far from being smooth. For the simulated geometry of the clumpy torus, only the Fe  $K\alpha$ /Si  $K\alpha$  ratio of the Circinus galaxy is close to the  $N = 5$  simulation results. For the other sources, the measured ratios are all below the simulation curve for  $N = 2$ .

#### 4 CONCLUSION AND DISCUSSION

X-ray fluorescent lines are unique features of the reflection spectrum of the torus around AGN, and can be relatively easily detected for obscured type II AGN. The spectral shape of the reflection spectrum depends on the fraction of photons that can

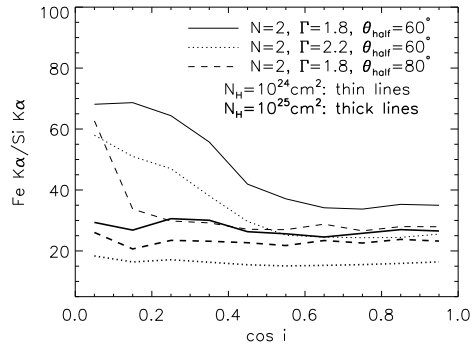


**Figure 3.** The effects of the photon index  $\Gamma$  and the half-opening angle of the torus on the predicted Fe  $K\alpha$ /Si  $K\alpha$  ratio.

leak through the torus, and thus on the clumpiness of the torus. Therefore, X-ray fluorescent lines at different energies can be used to probe the clumpiness of the torus. We have analysed a sample of type II AGN observed with *Chandra* HETGS and measured the fluxes for the Si  $K\alpha$  and Fe  $K\alpha$  lines. The measured Fe  $K\alpha$ /Si  $K\alpha$  ratios span a range between 5 – 60. These ratios are far smaller than the simulated values for smooth tori, indicating that the tori of the samples have clumpy distributions, rather than smooth ones.

Compared with the simulation results of clumpy tori, the Circinus galaxy has a Fe  $K\alpha$ /Si  $K\alpha$  ratio of  $\sim 60$ , which is close to the values of the  $N = 5$  simulation. The Fe  $K\alpha$ /Si  $K\alpha$  ratios of the other sources are all below the results of the  $N = 2$  simulation. This implies a very clumpy distribution for the torus. Below we discuss several factors that can affect the simulation results.

A direct factor affecting the simulation results is the abundance pattern. Liu & Li (2014) adopted the solar abundances from Anders & Grevesse (1989), and no variable abundances are investigated. Recent studies have reduced the solar Fe abundance from  $4.68 \times 10^{-5}$  (number relative to H, Anders & Grevesse 1989) to  $\sim 3 \times 10^{-5}$  (e.g. Asplund et al. 2009). This will lead to a similar decrease in the predicted Fe  $K\alpha$ /Si  $K\alpha$  ratio if the current abundance pattern is assumed. Similarly, if the abundance ratio of Fe/Si is changed several times, the Fe  $K\alpha$ /Si  $K\alpha$  ratio will also change similarly.

Another uncertainty in the results is the photon index,  $\Gamma$ , which is fixed at 1.8 in Liu & Li (2014). For optically-thick material, the emission of fluorescent lines is proportional to the available number of photons that can ionize the corresponding K-shell electrons. The relative number of photons at the ionization edge of Si and Fe will be increased for a large  $\Gamma$ . To test the effect of  $\Gamma$ , we re-run the  $N = 2$  simulation using a  $\Gamma$  of 2.2. The results for  $N_H = 10^{24} \text{ cm}^{-2}$  and  $10^{25} \text{ cm}^{-2}$  are plotted in Fig. 3 as dotted lines. As can be seen, for  $N_H = 10^{25} \text{ cm}^{-2}$ , the Fe  $K\alpha$ /Si  $K\alpha$  ratios are reduced by a factor of  $\sim 1.7$ , just as expected for optically-thick material. For  $N_H = 10^{24} \text{ cm}^{-2}$ , the material is not optically-thick for Fe K-shell ionization yet, and the reduction in the ratio is less than the prediction for optically-thick material.

Another unexplored effect is the half-opening angle (or covering factor), which is fixed to be  $60^\circ$ . In principle, a smaller covering factor will allow more photons to reach the observer, since it means less obscuration by the front-side torus gas. The effect on soft photons would be more significant due to their larger absorption cross-sections. Thus, smaller Fe  $K\alpha$ /Si  $K\alpha$  ratios would be expected for

smaller covering factors. To test the effect of covering factor, we also re-run the  $N = 2$  simulation by adopting a half-opening angle of  $80^\circ$ , the results of which are plotted in Fig. 3 as dashed lines. For  $N_{\text{H}} = 10^{24} \text{ cm}^{-2}$ , the Fe  $K\alpha$ /Si  $K\alpha$  ratio can be decreased by a factor of 2 for edge-on angles when using a half-opening angle of  $80^\circ$ . For  $N_{\text{H}} = 10^{25} \text{ cm}^{-2}$ , the effect of changing the half-opening angle is less significant, due to severe absorption and the isotropic nature of the emission.

We note that the simulated column densities ( $10^{24}$  and  $10^{25} \text{ cm}^{-2}$ ) are not matched exactly with the observed ones of the torus that were determined from the smooth torus models, which are shown here to be invalid. It seems that by including all these factors and with a clumpy torus of  $N \sim 2$  or smaller, the measured relatively low Fe  $K\alpha$ /Si  $K\alpha$  ratios ( $\sim 7$ ) can be obtained, without resort to abnormally low Fe/Si abundances. Current simulations of clumpy tori are limited by the crude grid and fixed abundances, geometry, and photon spectrum. It is clear that a fittable clumpy model, including the effects of  $N_{\text{H}}$ ,  $\Gamma$ , variable abundances and covering factors, is needed to fully understand the X-ray spectra of obscured AGN and to constrain the clumpiness of the torus. Such a model will be presented in a future work.

The simulation of Liu & Li (2014) assumed that both the Fe  $K\alpha$  and Si  $K\alpha$  photons are from the same torus, with the Si  $K\alpha$  photons from a thinner layer due to the larger absorption section at lower energy. In principle, the Si  $K\alpha$  photons can arise from physically distinct clouds with  $N_{\text{H}} \sim 10^{22} \text{ cm}^{-2}$ , for which the Fe  $K\alpha$ /Si  $K\alpha$  ratio is reduced significantly. For sources with  $N_{\text{H}} > 10^{24} \text{ cm}^{-2}$  and a covering factor  $\sim 0.5$ , the contribution of the Si  $K\alpha$  photons from distinct clouds with  $N_{\text{H}} \sim 10^{22} \text{ cm}^{-2}$  is unlikely to be significant, since the intensity of Si  $K\alpha$  photons increases with column density until saturated for large optical depth. For the extreme case that clouds with  $N_{\text{H}} \sim 10^{22} \text{ cm}^{-2}$  cover another half sky, the reduction of the Fe  $K\alpha$ /Si  $K\alpha$  ratio can not be larger than 50%. Nevertheless, the possibility of the origin of Si  $K\alpha$  photons from distinct clouds could be important for sources with  $N_{\text{H}} \sim 10^{23} \text{ cm}^{-2}$ .

Considering the contamination by the Mg XII Ly $\beta$  line to the Si  $K\alpha$  line, the relatively isolated S  $K\alpha$  line at 2.3 keV would be a better probe. However, due to the quick decline of the effective area of HEG around 2 keV, we found the S  $K\alpha$  line is only detectable in Circinus, Mrk 3, and NGC 1068, and the flux is similar to that of the Si  $K\alpha$  line. Nevertheless, the effective area around S, Ar, and Ca  $K\alpha$  lines would be improved for the soft X-ray calorimeter on-board Astro-H, which would also enable a much larger sample of obscured AGN. The results show that non-Fe fluorescent lines are a potentially powerful probe of the clumpiness of the torus around AGN.

## ACKNOWLEDGEMENTS

We thank our referee Franz Bauer for pointing out the possible distinct origin of Si  $K\alpha$  photons and other valuable suggestions. We also thank Richard Long for a careful reading of the manuscript. JL is supported by NSFC grant 11203032 and YL supported by NSFC grant 11573027. This research is based on data obtained from the *Chandra* Data Archive.

## REFERENCES

- Anders, E. & Grevesse, N. 1989, *Geochimica et Cosmochimica Acta*, 53, 197
- Antonucci, R. 1993, *ARA&A*, 31, 473
- Arévalo, P., Bauer, F. E., Puccetti, S., et al. 2014, *ApJ*, 791, 81
- Asplund, M., Grevesse, N., Sauval, A. J., Scott, P. 2009, *ARA&A*, 47, 481
- Baloković, M., Comastri, A., Harrison, F. A., et al. 2014, *ApJ*, 794, 111
- Bauer, F. E., Arévalo, P., Walton, D. J., et al. 2015, *ApJ*, 812, 116
- Bianchi, S., Maiolino, R., & Risaliti, G. 2012, *Advances in Astronomy*, 2012, 782030
- Braito, V., Reeves, J. N., Sambruna, R. M., Gofford, J. 2011, *MNRAS*, 414, 2739
- Canizares, C. R., Davis, J. E., Dewey, D., et al. 2005, *PASP*, 117, 1144
- Comastri, A. 2004, *ASSL*, 308, 245
- Elitzur, M. 2008, *NewAR*, 52, 274
- George, I. M. & Fabian, A. C. 1991, *MNRAS*, 249, 352
- Grandi, P., Guainazzi, M., Cappi, M., Ponti, G. 2007, *MNRAS*, 381, L21
- Hönig, S. F. 2013, Packham, C., Mason, R., and Alonso-Herrero, A., eds, *Proc. of the Torus Workshop 2012*, Univ. Texas, San Antonio, arXiv:1301.1349
- Huenemoerder, David P., Mitschang, A., Dewey, D., et al. 2011, *AJ*, 141, 129
- Kaastra, J. S. & Mewe, R. 1993, *A&AS*, 97, 443
- Kalberla, P. M. W., Burton, W. B., Hartmann, D., Arnal, E. M., Bajaja, E., Morras, R., Poppel, W. G. L. *Astronomy & Astrophysics*, 440, 775
- Kinkhabwala, A., Behar, E., Sako, M., Gu, M. F., Kahn, S. M., Paerels, F. B. S. 2003, arxiv: astro-ph/0304332
- Koss, M. J., Romero-Cañizales, C., Baronchelli, L., et al. 2015, *ApJ*, 807, 149
- Krolik, J. H. & Begelman, M. C. 1988, *ApJ*, 329, 702
- Liu, J. 2016, submitted to *MNRAS*
- Liu, Y. & Li, X. 2014, *ApJ*, 787, 52
- Levenson, N. A., Krolik, J. H., Zycki, P. T., Heckman, T. M., Weaver, K. A., Awaki, H., Terashima, Y. 2002, *ApJL*, 573, 81
- Marinucci, A., Bianchi, S., Matt, G., Alexander, D. M., Baloković, M., Bauer, F. E., Brandt, W. N., Gandhi, P., et al. 2016, *MNRAS*, 456, L94
- Marinucci, A., Risaliti, G., Wang, J., Bianchi, S., Elvis, M., Matt, G., Nardini, E., Braito, V. 2013, *MNRAS*, 429, 2581
- Markowitz, A. G., Krumpke, M., & Nikutta, R. 2014, *MNRAS*, 439, 1403
- Matt, G., Fabian, A. C., Reynolds, C. S. 1997, *MNRAS*, 289, 175
- Matt, G.; Bianchi, S.; Guainazzi, M.; Molendi, S., 2004, *A&A*, 414, 155
- Molendi, S.; Bianchi, S.; Matt, G., 2003, *MNRAS*, 343, L1
- Murphy, K. D. & Yaqoob, T. 2009, *MNRAS*, 397, 1549
- Nandra, K. & George, I. M. 1994, *MNRAS*, 267, 974
- Netzer, H. 2015, *ARA&A*, 53, 365
- Risaliti, G., Elvis, M., Fabbiano, G., et al. 2007, *ApJL*, 659, 111
- Rivers, E., Baloković, M., Arévalo, P., et al. 2015, *ApJ*, 815, 55
- Reynolds, C. S., Fabian, A. C., Makishima, K., Fukazawa, Y., Tamura, T. 1994, *MNRAS*, 268L, 55
- Sambruna, R. M., Reeves, J. N., Braito, V. 2007, *ApJ*, 665, 1030
- Shirai, H., Fukazawa, Y., Sasada, M., et al. 2008, *PASJ*, 60, 263
- Shu, X. W., Yaqoob, T., Wang, J. X. 2011, *ApJ*, 738, 147
- Xu, W.; Liu, Z.; Gou, L.; Liu, J. 2016, *MNRAS*, 455, L26

Yaqoob, T. & Murphy, K. D. 2011, *MNRAS*, 412, 1765

Yaqoob, T. 2012, *MNRAS*, 423, 3360

Yaqoob, T., Tatum, M. M., Scholtes, A., Gottlieb, A., & Turner,  
T. J. 2015, *MNRAS*, 454, 973